ORIGINAL PAPER

An Experimental Study on Porosity and Permeability Stress-Sensitive Behavior of Sandstone Under Hydrostatic Compression: Characteristics, Mechanisms and Controlling Factors

Chengyuan Xu[1] · Chong Lin[1] · Yili Kang[1] · Lijun You[1]

Abstract

Porosity and permeability stress-sensitive behavior of sandstone is investigated through porosity and permeability measurements under hydrostatic compression. An empirical logarithm model is applied to the evaluation of stress sensitivity. Mercury injection, casting thin sections and scanning electron microscope are adopted to discuss the microscopic controlling factors and mechanisms of stress-sensitive behavior of sandstone. Disparities between laboratory-scale and field-scale data are also discussed. Experimental results show that both porosity and permeability decrease with increasing effective stress, and permeability is more sensitive to stress. The evolution of porosity and permeability with increasing effective stress follows the logarithmic model and can be classified into three stages: rapid decline, moderative decline and stable-slight decline stage. Stronger permeability stress sensitivity is observed in specimens with lower initial porosity and permeability, which is fundamentally controlled by the size and shape of void spaces as well as the content and distribution of soft minerals. While porosity stress sensitivity is observed to be discrete. Pore throat with small aspect ratio and irregular shape, fractures and minerals with lower elasticity modulus lead to the increase in permeability stress sensitivity of sandstone. The stress sensitivity characteristics are essentially the result of the dissimilar deformation responses of pores and framework grains under effective stress. Stress sensitivity evaluated in the laboratory usually does not completely represent the stress sensitivity in the field, due to stress release, drilling induced fractures and the difference of experimental and in situ conditions.

Keywords Sandstone · Stress-sensitive behavior · Porosity and permeability · Effective stress · Microstructure

List of symbols

C_c	Compressibility of circular pore
C_e	Compressibility of elliptical pore
C_p	Compressibility of penny-shape pore
E	Young's modulus
K	Permeability
K_0	Permeability at effective stress σ_0
K_0'	Permeability at terminal stress during the loading and unloading cycle
K_i	Permeability at effective stress σ_i
n_k	Effective stress coefficient
P_c	Confining pressure
P_f	Flow pressure
P_p	Pore pressure
r	Pore radius
R^2	Coefficient of determination
S_s	Stress sensitivity coefficient
w	Fracture width
α	Porosity sensitivity exponent
γ	Pressure sensitivity coefficient
ε	Aspect ratio of pore
σ	Effective stress
σ_0	Effective stress at initial measured point
σ_i	Effective stress at a certain measured point
ν	Poisson's ratio
ϕ	Porosity
ϕ_0	Porosity at effective stress σ_0
ϕ_i	Porosity at effective stress σ_i

✉ Yili Kang
  cwct_fdc@163.com

[1] State Key Laboratory of Oil and Gas Reservoir Geology
   and Exploitation, Southwest Petroleum University, No.8
   Xindu Avenue, Xindu District, Chengdu 610500, China

2322

C. Xu et al. (2018) 51:2321–2338

1 Introduction

Reservoir rock is a typical porous medium composed of framework grains and void spaces. Variations in the in situ stress state cause the change in flow paths including pores, throats and fractures, which further result in the variations of porosity and permeability (Geertsma 1957; Ostensen 1986). Wellbore drilling upsets the balance of in situ stresses, and the stress state continues to change during the subsequent operations, including cementation, completion, workover, hydraulic fracturing and production. This commonly leads to the dynamic variation of reservoir porosity and permeability as well as some unfavorable effects on oil and gas exploration and development, such as working fluid loss, reserve evaluation error and well productivity decline (Vairogs et al. 1971; Archer 2008; Lei et al. 2008; Kang et al. 2015; Xu et al. 2016, 2017, 2018). Therefore, the understanding of the stress-sensitive behavior of reservoir rock porosity and permeability plays a significant role in the oil and gas industry.

The impacts of stress on reservoir permeability were firstly reported by Fatt and Davis in 1950 s. Sandstone samples experienced an 11–41% reduction of permeability under increasing confining pressure (Fatt and Davis 1952). Since then, a series of laboratory experiments aiming at the simulation of in situ stress change were conducted to investigate the variations in porosity/permeability under varying stress. Stress types include confining pressure (Dong et al. 2010), pore pressure (Berumen and Tiab 1996), uniaxial pressure (Dautriat et al. 2009) and triaxial pressure (Han et al. 2016). Subsequently, the evolution of porosity and permeability with stress under cyclic loading was experimentally studied by Wang et al. (2017). Xu and Yang (2016) and Liu et al. (2016) carried out triaxial creep tests to investigate the evolutions of permeability in granite gneiss and sandstone, respectively. Data from different experimental methods were widely compared and discussed (Al-Wardy and Zimmerman 2004; Ghabezloo et al. 2009). Empirical or theoretical mathematic models between porosity/permeability and stress were obtained to evaluate and predict the stress-sensitive behavior of porosity and permeability. Some well-known models include the power model (Shi and Wang 1986), exponential model (Louis 1972), binomial model (Seeburger and Amos 1984; Jaeger et al. 2007), third-order polynomial model (Worthington 2008) and logarithm model (Jones and Owens 1980; Walsh 1981). To obtain a more precise picture of this stress-sensitive behavior, modified models were developed based on a broad theoretical background, such as the capillary buddle model (Tian et al. 2015a; Ma and Wang 2016), two-part Hooke's model (TPHM) (Zheng et al. 2015), micromechanical model (Dormieux et al. 2011) and Hertzian contact theory model (Zhang et al. 2014).

The impact factors on rock stress sensitivity have also been widely examined. Rock specimens with lower initial porosity and permeability are more sensitive to stress (Kilmer et al. 1987). This was attributed to a complex seepage system consisting of microfractures and narrow throats (Clarkson et al. 2012; Shapiro et al. 2015), both of which were considered to be easier to compact. Furthermore, fractures with a small aspect ratio can significantly enhance rock stress sensitivity (Brower and Morrow 1985; Huo et al. 2014). Rock microstructures were characterized by mercury injection tests, casting thin sections, a scanning electron microscope (SEM), micro-CT, 3D laser scanner and nuclear magnetic resonance (NMR). The geometry, scale, quantity and distribution of pores, throats and fractures, which are affected by the diagenetic processes, are related to the stress-sensitive behavior of the rock (Farquhar et al. 1993; Li et al. 2013; Vogler et al. 2016; Xiao et al. 2016; Zhang et al. 2016). In addition to the above structural factors, mineral also plays an important role in the stress-sensitive behavior, due to their varying deformation properties under loading (Bruno et al. 1991; Al-Wardy and Zimmerman 2004). The effects of size, array, contact types and sorting of grains on rock stress-sensitive behavior were investigated by Zhang et al. (2014). Rock stress-sensitive behavior is also believed to be partly affected by environmental factors, such as mechanical loading path and ambient temperature (Nguyen et al. 2014; Santos et al. 2014; Meng et al. 2015). Other researchers have focused on the influences of water saturation (Thomas and Ward 1972; Fu et al. 2015), flowing fluid type (Qi et al. 2013) and working fluid immersion (Kang et al. 2016; Li et al. 2017a). Fines release (Zhang 2013) and the proppant effect (Kassis and Sondergeld 2010; Li et al. 2017b) were examined as well.

Although numerous of studies on the porosity and permeability stress sensitivity of sandstone have been published based on laboratory tests and numerical simulations, the effects of microstructure and deformation characteristics on the stress-sensitive behavior of porosity and permeability of sandstone are still unclear and require further investigation. In the current paper, a series of laboratory experiments are conducted to measure the porosity and permeability of sandstones with a wide range of permeability under a cyclic confining stress. Then, the stress-sensitive behavior of porosity and permeability is analyzed based on the experimental results and evaluated by fitting an empirical logarithmic model. Next, the effect of microstructure on the stress-sensitive behavior of porosity and permeability is analyzed based on microscopic observations of sandstone. Mechanisms of stress-sensitive behavior are revealed according to the deformation properties of pores, throats, fractures and minerals. Finally, the discrepancy of stress-sensitive behavior between laboratory-scale and field-scale is discussed.

2 Methodology

2.1 Materials

Sandstone samples cored from the Silurian formation of Tarim Basin in northwestern China were selected for the current study. Samples are fine-medium-grained lithic quartz sandstones buried 5370–5680 m underground. Porosity ranges from 2.35 to 20.5%, and permeability ranges from 4.5×10^{-17} to 2.071×10^{-12} m^2 (measured under 3 MPa confining pressure and 0.7 MPa flowing pressure by pure nitrogen). The Silurian sandstone is dominated by quartz (86%) with minor amount of clay minerals (11%) and calcite (3%). Clay minerals are composed of a mixture of illite (54%), kaolinite (32%), chlorite (7%) and interstratified illite/montmorillonite (7%). Samples were cut cylindrically into specimens approximately 2.5 cm in diameter and 3–6 cm in length, and the ends were polished smooth (Fig. 1). A tensile fracture parallel to the specimen's main axis was created using the Brazilian splitting test for artificially fractured specimen. Pretreatment with toluene and methanol was conducted to remove oil and salt. Specimens were dried in the homo-thermal oven at 60 °C for 48 h and stored in drying vessel. The basic parameters of the sandstone specimens are shown in Table 1.

2.2 Porosity and Permeability Stress Sensitivity Test

A CMS-300 core measurement system was used to measure the sandstone porosity and permeability under various confining pressures (P_c) at a constant flowing pressure (P_f). The system performed instrument calibration to calculate the space volume of the system, and the pressure sensors

Fig. 1 Typical sandstone specimens from the Silurian formation of Tarim Basin in northwestern China

were reset to zero. An integrated digital caliper workstation automatically measured specimen dimensions, made corrections for irregularly shaped specimens and calculated apparent volume of the specimen. According to Boyle's law, the product of pressure and volume is a constant for a given mass of ideal gas if the temperature remains unchanged within a closed system. During the measurement, the system temperature was constant 25 °C and the high purity dry nitrogen gas (99.9%) was assumed as ideal gas. Then, a container of known volume was pressure equilibrated with the specimen. After pressure equilibrium, the pore volume can be calculated based on the Boyle's Law and the advanced calibration techniques. Porosity with a range from 0.01 to 40% can be obtained by the ratio of pore volume to apparent volume. The absolute error of the porosity determination by the system is 0.01%.

A liquid film flowmeter and a gas flowmeter are assembled in the system. The measurement range of these two flowmeters is 1.67×10^{-11}–8.33×10^{-9} and 8.33×10^{-9}–8.33×10^{-4} m^3/s, respectively. The system can automatically choose the flowmeter according to flow rate. Liquid film flowmeter is enabled when flow rate is less than 8.33×10^{-9} m^3/s, and gas flowmeter is enabled when flow rate is larger than 8.33×10^{-9} m^3/s. An integrated form of the combined Darcy, Klinkenberg and Forchheimer equations was used to accurately determine the permeability range from 5×10^{-20} to 1.5×10^{-11} m^2 with the relative error of 5%. The system can correct the influence of the gas slippage effect on the directly measured apparent gas permeability based on Klinkenberg equation. The intrinsic permeability under a specific confining pressure is obtained based on the regression analysis between the gas permeability and the reciprocal of the mean pressure. The inlet pressure was set to 0.1–1.0 MPa according to the initial permeability of the specimen, and the outlet pressure was equal to the atmosphere pressure (0.1 MPa). According to Yang et al. (2017), as the various inlet pressures were small and close to each other, the effect of effective stress was little and can be ignored in the determination of Klinkenberg corrected permeability. Confining pressure ranging from 3 to 65 MPa was applied and removed in a cyclic way. The specimen was held under hydrostatic compression during the experiments. The effective stress is calculated by Eq. 1.

$$\sigma = P_c - n_k P_p \tag{1}$$

where σ, P_c, P_p and n_k are the effective stress, confining pressure, pore pressure and effective stress coefficient, respectively. n_k has an average value of 0.55 according to the triaxial test. To simplify the calculation, n_k is assumed to be 1 in the current paper. Then, the effective stress can be expressed as

$$\sigma = P_c - P_p \tag{2}$$

2324

C. Xu et al. (2018) 51:2321–2338

Table 1 Basic physical parameters of sandstone specimens

Permeability magnitude	No.	Burial depth (m)	Length (cm)	Diameter (cm)	Porosity (%)	Permeability (m²)
10^{-17} m²	TY1	5595.27	3.93	2.56	2.62	4.5×10^{-17}
	TY3	5589.38	3.33	2.56	3.15	5.6×10^{-17}
	TY4	5567.63	3.77	2.54	2.67	5.9×10^{-17}
	TY2	5569.30	3.27	2.54	2.35	7.3×10^{-17}
10^{-16} m²	TY9	5570.89	3.81	2.54	4.30	2.82×10^{-16}
	TY5	5678.45	4.94	2.47	6.94	3.11×10^{-16}
	TY6	5586.62	5.72	2.48	5.84	4.56×10^{-16}
10^{-15} m²	TY7	5583.19	4.01	2.56	4.02	1.05×10^{-15}
	TY8	5588.20	3.72	2.56	3.29	1.09×10^{-15}
	TY10	5585.53	3.74	2.56	6.55	1.68×10^{-15}
	TY11	5581.30	3.62	2.56	7.62	1.84×10^{-15}
	TY12	5576.85	3.49	2.55	8.81	4.60×10^{-15}
10^{-14} m²	TY13	5396.68	3.67	2.53	9.86	1.01×10^{-14}
	TY14	5411.74	3.60	2.53	13.37	2.04×10^{-14}
	TY15	5392.40	3.65	2.52	11.70	2.14×10^{-14}
	TY16	5387.85	4.38	2.52	11.95	4.91×10^{-14}
10^{-13} m²	TY17	5383.39	3.39	2.56	13.12	1.02×10^{-13}
	TY18	5373.57	3.66	2.55	14.66	1.04×10^{-13}
	TY19	5386.16	4.35	2.52	15.53	1.43×10^{-13}
	TY20	5375.07	3.39	2.55	16.64	1.70×10^{-13}
	TY21	5387.85	4.84	2.52	17.23	3.40×10^{-13}
10^{-12} m²	TY22	5384.12	2.54	2.51	17.98	1.256×10^{-12}
	TY23	5383.57	2.72	2.51	17.16	1.649×10^{-12}
	TY24	5379.93	3.56	2.56	16.81	1.680×10^{-12}
	TY25	5375.62	3.84	2.55	20.50	2.071×10^{-12}
Artificially fractured specimen	TY26F	5678.45	4.94	2.47	7.14	1.602×10^{-14}
	TY27F	5586.62	5.72	2.48	7.30	7.753×10^{-15}

2.3 Microstructural Observations

Mercury injection, casting thin sections and SEM were conducted for the quantitative and qualitative investigation of the microstructural properties of the sandstone samples. These experimental samples for the microstructural observations were taken from the same sandstone for the stress sensitivity tests. The above microstructural observations were conducted on Poremaster60 automatic mercury porosimeter, LV100Po multi-view transflective polarizing microscope and Quanta 450 environmental scanning electron microscope, respectively. Pore throat radius distribution, permeability devotion of pore throat radius, casting thin sections images and SEM images were obtained to characterize the microstructure of the sandstone samples.

3 Experimental Results

3.1 Stress-Sensitive Behavior of Porosity

Figure 2 shows the experimental results of porosity stress-sensitive behavior. The porosity is normalized to highlight the variation. It can be seen that porosity declines with increasing effective stress. The decreasing rates are larger during the lower effective stress range (3–15 MPa). This rate starts to decrease when the effective stress exceeds 15 MPa and remain almost stable for effective stress above 20 MPa. The variation in porosity with increasing effective stress can be divided into three stages: rapid decline, moderative decline and stable-slight decline stage. The demarcation points exist between 15–20 MPa. Specimens
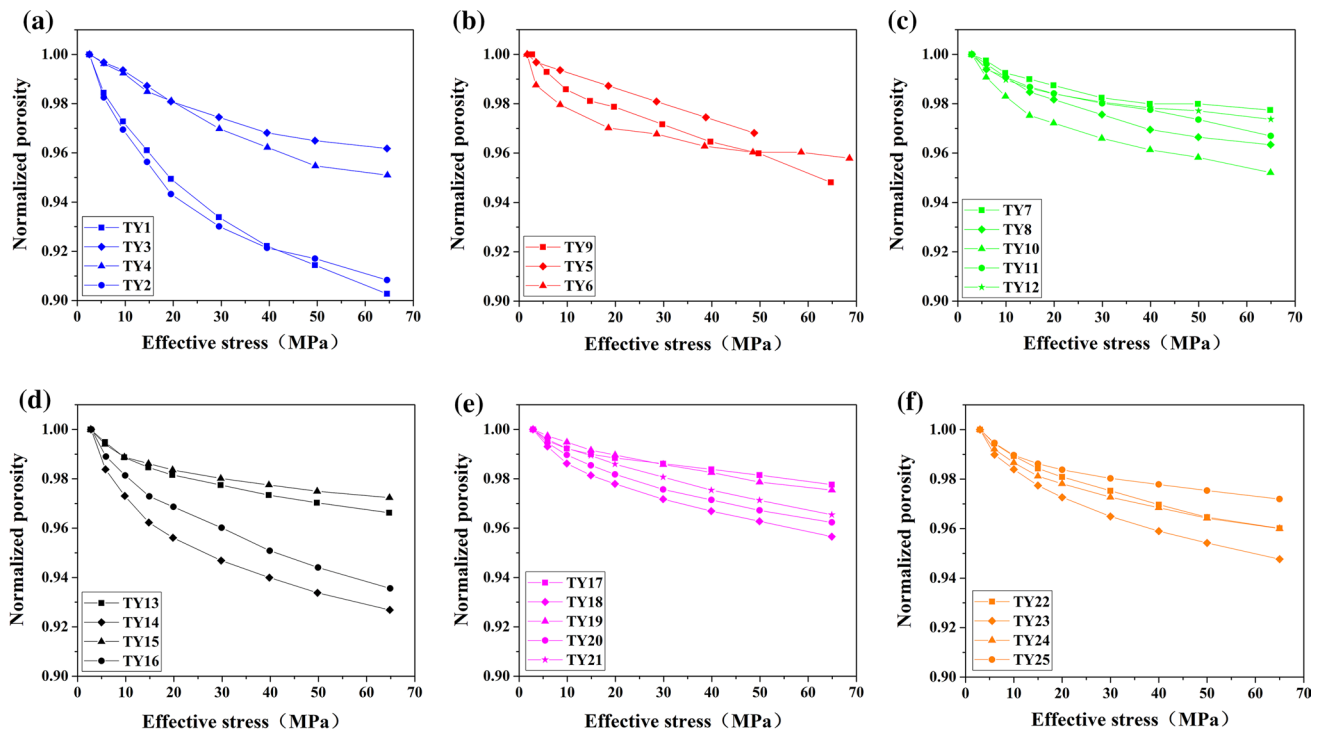
Fig. 2 Porosity changes in sandstone specimens with different permeability magnitudes with effective stress: **a** 10^{-17} m²; **b** 10^{-16} m²; **c** 10^{-15} m²; **d** 10^{-14} m²; **e** 10^{-13} m²; **f** 10^{-12} m²

with the same permeability magnitude show similar porosity stress-sensitive behavior, except specimens with the permeability magnitudes of 10^{-17} and 10^{-14} m². The porosity stress-sensitive behavior of specimens with these two permeability magnitudes is quite different (see Fig. 2a, TY1, TY2 and TY3, TY4; Fig. 2d, TY13, TY15 and TY14, TY16), which are attributed to microstructural differences. This can be demonstrated using the γ/α ratio (γ and α denotes pressure sensitivity coefficient and porosity sensitivity exponent, respectively) developed by David et al. (1994), which relates to the pore compressibility and reflects the rock microstructure. Higher γ/α ratio indicates a relatively more compressible pore space and is inversely proportional to the crack aspect ratio. Therefore, the high γ/α ratio in low porosity rocks is probably a manifestation of the crack closure processes. γ/α values for specimens TY1, TY2, TY3, TY4 are 0.0055, 0.008, 0.0022, 0.0033 MPa^{-1}, respectively. The γ/α of the first two specimens are similar and are significantly different from that of the last two specimens (with similar γ/α). Therefore, the microstructure of the two groups of specimens is similar within the group and markedly different between the groups. A similar conclusion can be drawn for Fig. 2d, because γ/α values for specimens TY13, TY15, TY14, TY16 are 0.0005, 0.0004, 0.0012, 0.0010 MPa^{-1}, respectively. When the maximum effective stress of 65 MPa is exerted, the porosity decline for all specimens is about 2.23–9.73%, with no obvious relation to initial porosity.

3.2 Stress-Sensitive Behavior of Permeability

Experimental results of permeability stress sensitivity are presented in Fig. 3. Similar to porosity, permeability also decreases with increasing effective stress. The decreasing rates (defined as dK/dσ) of permeability for intact specimens in the lower effective stress range (3–15 MPa) are much larger than those in the higher effective stress range, which are almost constant. Compared with the intact specimens, artificially fractured specimens show much larger decreasing rates for effective stress below 15 MPa. The turning point is around 20 MPa for intact specimens and around 5–15 MPa for artificially fractured specimens. The decreasing rates are larger before the turning points. After the turning point, the permeability declines more slowly. Unlike porosity, specimens with the same permeability magnitude show greatly different stress-sensitive behavior, which indicates that permeability is more sensitive to microstructure (especially the connectivity of pores) than porosity. About 3.37–99.99% of the initial permeability is lost at the maximum effective stress of 65 MPa. The percent of lost permeability shows a negative correlation with initial permeability, which will be discussed in later Sect. 4.1.

During the unloading process, the permeability increases with decreasing effective stress. Although the unloading curvilinear paths are similar to the loading process, all specimens display hysteretic behavior between unloading
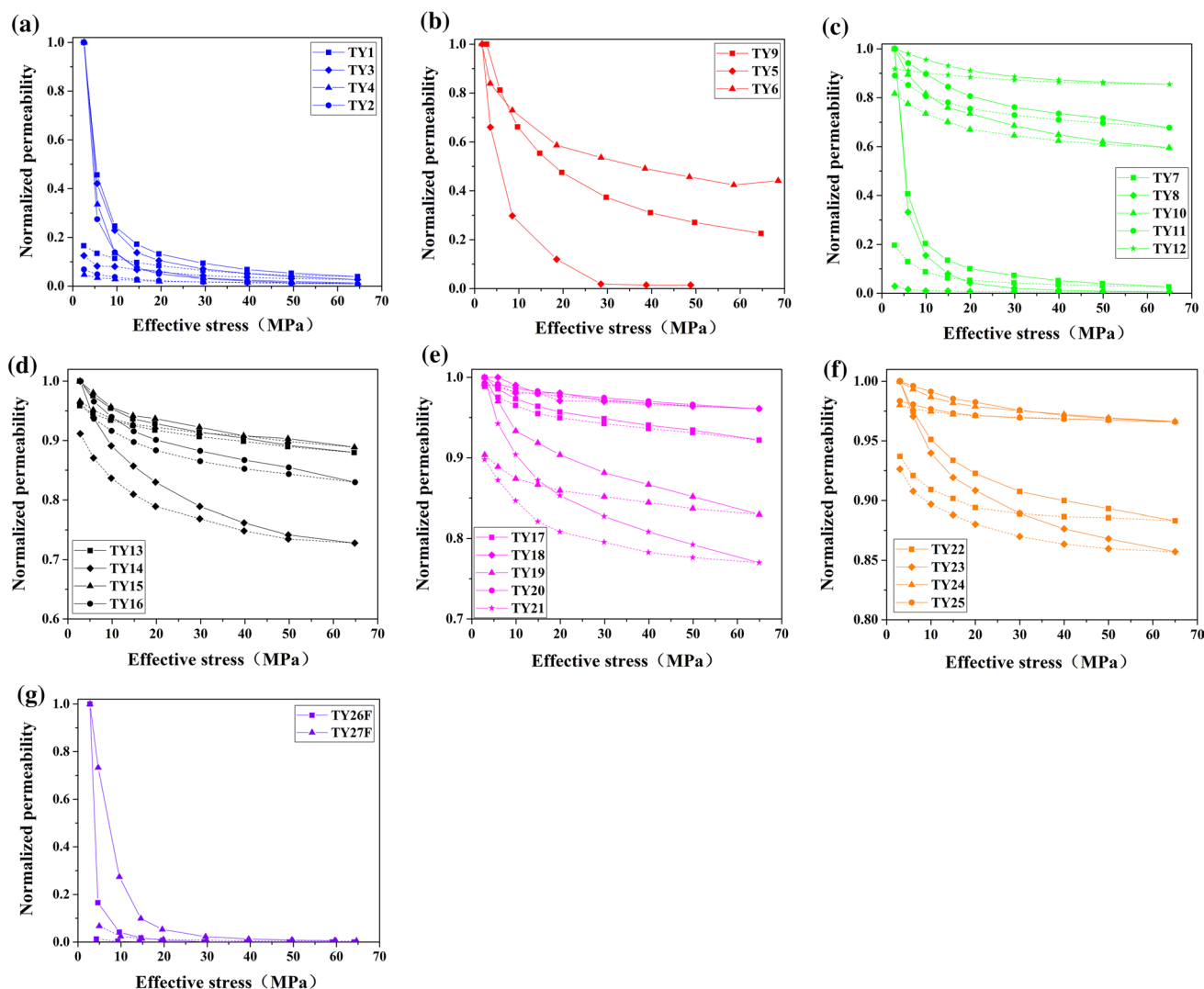
2326

C. Xu et al. (2018) 51:2321–2338

Fig. 3 Permeability changes in sandstone specimens with different permeability magnitudes with effective stress: **a** 10^{-17} m^2; **b** 10^{-16} m^2; **c** 10^{-15} m^2; **d** 10^{-14} m^2; **e** 10^{-13} m^2; **f** 10^{-12} m^2; **g** artificially fractured specimen (Loading is solid line, and unloading is dashed line.)

and loading curves (Fig. 3a–g). 2.92–99.29% of the initial permeability is recovered after the unloading process. This apparent hysteresis depends on stress history of the specimen. However, it does not mean that the loss of permeability is irreversible. The loading curve can be reproduced after the specimen is put at ambient conditions for a sufficient time. As the deformation which changes the permeability is mainly elastic in most laboratory experiments, the contribution of plastic deformation is fairly small, which has been widely confirmed in previous studies (Thomas and Ward 1972). It is noteworthy that the permeability stress-sensitive behavior of some intact specimens with permeability below 10^{-14} m^2, such as TY1, TY2, TY3, TY4, TY5, TY7 and TY8, is similar to that of the artificially fractured specimens. These intact specimens all show strong stress sensitivity. Sandstone with strong stress sensitivity generally has

microfractures or fracture-like pores, while the sandstone with weak stress-sensitive usually has well-connected pores (Xiao et al. 2016; Davies and Davies 2001). It indicates that the flow paths in low permeability specimens are mainly microfractures or fracture-like pores (Ostensen 1983).

3.3 Evaluation of Stress Sensitivity

In attempting to compare porosity and permeability sensitivity of different specimens and controlling factors, a satisfactory evaluation criterion of stress sensitivity must be addressed first. An empirical logarithmic model proposed by Jones and Owens (1980) and theoretically derived by Walsh (1981) is selected to evaluate the stress sensitivity for various porosities and permeabilities. The stress sensitivity

is evaluated by the stress sensitivity coefficient S_s which is described in Eq. 3.

$$S_s = \frac{1 - \left(K_i/K_0\right)^{1/3}}{\log\left(\sigma_i/\sigma_0\right)} \tag{3}$$

where S_s is the stress sensitivity coefficient. σ_i and σ_0 are effective stress at a certain and initial measured point. K_i and K_0 are measured permeability at effective stress σ_i and σ_0, respectively. Porosity stress sensitivity also can be evaluated using Eq. 3 by replacing K_i and K_0 with ϕ_i and ϕ_0, respectively.

The applicability and evaluation standard of this criterion have been exhaustively discussed (Jones and Owens 1980; Xiao et al. 2016). Linear regression analysis through the least squares method is applied to determine the stress sensitivity coefficient.

The stress sensitivity coefficient and corresponding coefficient of determination (R^2) of loading porosity, loading permeability and unloading permeability are listed in Table 2. R^2 for most specimens is larger than 0.90, and

only 3 specimens show R^2 between 0.70–0.90. The high value of R^2 indicates the experimental data fit well with Eq. 3, and the stress sensitivity coefficient obtained from the selected evaluation criterion is credible. The stress sensitivity coefficient of porosity is 0.005–0.0218, with an average R^2 of 0.9605. The stress sensitivity coefficient of permeability during loading process is 0.0081–0.8069, with an average R^2 of 0.9603. The stress sensitivity coefficient of permeability during unloading process is 0.0036–0.6896, with an average R^2 of 0.9602.

4 Discussion

4.1 Controlling Factors of Sandstone Stress Sensitivity

4.1.1 Initial Porosity and Permeability

In this section, this relationship between the permeability stress sensitivity and the initial porosity and permeability

Table 2 Stress sensitivity coefficient of specimen

No.	Loading				Unloading	
	S_s of porosity	R^2	S_s of permeability	R^2	S_s of permeability	R^2
TY1	0.0215	0.9586	0.5076	0.9482	0.2557	0.9700
TY3	0.0082	0.9004	0.5419	0.9423	0.2770	0.9766
TY4	0.0102	0.8678	0.6243	0.8751	0.2636	0.9886
TY2	0.0218	0.9868	0.6337	0.8772	0.3424	0.9981
TY9	0.0104	0.9214	0.2710	0.9862	0.2340	0.9886
TY5	0.0059	0.9203	0.5379	0.9776	–	–
TY6	0.0090	0.9865	0.1539	0.9939	–	–
TY7	0.0054	0.9703	0.5668	0.9122	0.3856	0.9764
TY8	0.0085	0.9586	0.6882	0.9197	0.3631	0.7705
TY10	0.0115	0.9955	0.1181	0.9989	0.0738	0.9921
TY11	0.0071	0.9527	0.0853	0.9842	0.0164	0.9514
TY12	0.0065	0.9985	0.0377	0.9778	0.0165	0.9520
TY13	0.0076	0.9807	0.0289	0.9950	0.0185	0.9716
TY14	0.0178	0.9978	0.0736	0.9960	0.0542	0.9972
TY15	0.0066	0.9973	0.0266	0.9907	0.0186	0.9889
TY16	0.0145	0.9645	0.0416	0.9915	0.0346	0.9942
TY17	0.0050	0.9780	0.0181	0.9863	0.0161	0.9942
TY18	0.0098	0.9757	0.0092	0.9313	0.0069	0.9224
TY19	0.0052	0.9149	0.0420	0.9896	0.0201	0.9958
TY20	0.0084	0.9588	0.0090	0.9819	0.0074	0.9761
TY21	0.0072	0.9063	0.0611	0.9991	0.0385	0.9916
TY22	0.0090	0.9551	0.0309	0.9967	0.0163	0.9535
TY23	0.0123	0.9808	0.0380	0.9979	0.0201	0.9952
TY24	0.0095	0.9895	0.0084	0.9982	0.0036	0.9964
TY25	0.0067	0.9960	0.0081	0.9608	0.0046	0.9871
TY26F	–	–	0.8069	0.7467	0.6896	0.8779
TY27F	–	–	0.6474	0.9721	0.5906	0.7989

2328

C. Xu et al. (2018) 51:2321–2338

Fig. 4 Relationship between the stress sensitivity coefficient and initial porosity and permeability of specimens
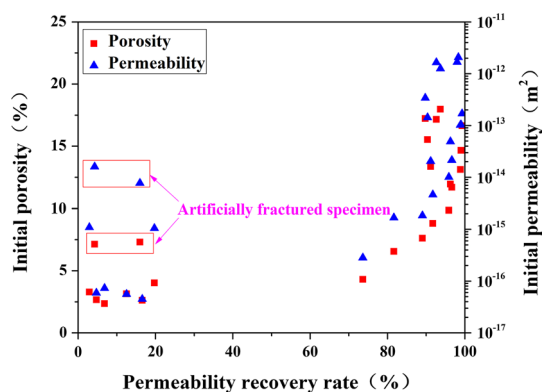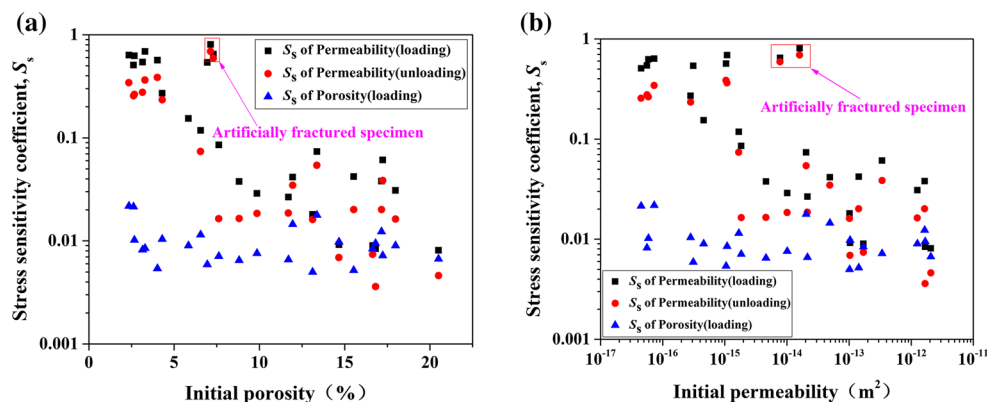

Fig. 5 Relationship between permeability recovery rate and initial porosity and permeability of specimens

is further discussed. The S_s versus initial porosity and permeability of specimens is illustrated in Fig. 4. The porosity S_s is very small (average value is about 0.01) and shows no relation with a specimen's initial porosity or permeability. However, the permeability S_s is much larger and ranges from 0.008 to 0.688, which decreases with increasing initial porosity and permeability. These results are consistent with most previous work (Fu et al. 2015). There are two apparent demarcation points at 10% of porosity and 10^{-14} m^2 of permeability. The permeability S_s of specimens with porosity below 10% is much higher than that of specimens with porosity above 10%. Similarly, the permeability S_s of specimens with permeability below 10^{-14} m^2 is much higher than that of specimens with permeability above 10^{-14} m^2, whose S_s is almost less than 0.1. When porosity is below 10% or permeability is below 10^{-14} m^2, the initial porosity and permeability have a strong effect on the permeability stress sensitivity. When porosity is above 10% or permeability is above 10^{-14} m^2, the effect of initial porosity and permeability is negligible. However, this conclusion does not apply for the artificially fractured specimens, which show a much higher S_s of permeability

than the intact specimens with similar initial porosity and permeability.

Permeability recovery rate, defined as the ratio of the permeability at terminal stress to the permeability at initial stress during the loading and unloading cycle (K_0'/K_0), is also related to initial porosity and permeability of the specimen (Fig. 5). Contrary to the permeability S_s, the permeability recovery rate raises with increasing initial porosity and permeability. The demarcation point appears at 12% of porosity and 10^{-14} m^2 of permeability. The permeability recovery rate of specimens with initial porosity or permeability before the demarcation point fluctuates between 90–100% and is much higher than that after the demarcation point. The permeability recovery rate after the demarcation point decreases rapidly with decreasing initial porosity and permeability. For artificially fractured specimens, the permeability recovery rate is much lower than that of intact specimens with similar initial porosity and permeability.

The great differences for permeability S_s and permeability recovery rate on both sides of the demarcation points are caused by the different responses of the pore structure to effective stress. For specimens with porosity below 10% or permeability below 10^{-14} m^2, microfractures and fracture-like pores make an important contribution to the permeability. The higher permeability S_s of these specimens is a manifestation of fracture-closure process, which is almost irreversible during unloading process. Therefore, the lower the initial porosity and permeability, the larger the contribution of microfractures and fracture-like pores to permeability, the higher the permeability S_s and the lower the permeability recovery rate. On the other hand, for the specimens with porosity above 10% or permeability above 10^{-14} m^2, their permeabilities are mainly dominated by pores and wide throats. The lower permeability S_s in these specimens is probably a manifestation of elastic pore compaction, which is relatively reversible during unloading process. Therefore, the larger the initial porosity and permeability, the larger the contribution of pores and wide throats to permeability, the

lower the permeability S_s and the higher the permeability recovery rate.

4.1.2 Micropores and Throats

In the previous section, the permeability S_s declines with increasing initial porosity and permeability. Porosity and permeability are a macroscopic reflection of microscopic pore structure. Therefore, the impact of initial porosity and permeability on stress sensitivity coefficient is essentially controlled by pore structure. Pores reflect the reservoir capacity of the rock, while the shape and size of the throats controls the permeability of the pores (Bernabé et al. 2003; Tian et al. 2015b). That is, permeability stress sensitivity is mainly the result of the deformation of interconnected void space.

Mercury injection experimental results (Figs. 6, 7) show that the distribution of pore throat radius is positively correlated with permeability. Higher porosity/permeability sample usually has larger pore throat size, including maximum, median and average pore throat radius (Fig. 6). The higher the sample permeability, the larger the pore throat size and the larger its contribution to permeability (Fig. 7). According to the analysis results in the previous section, it can be

concluded that a specimen with larger pore and throat usually leads to weaker stress sensitivity.

Figure 8 shows the microscopic pore structure of six specimens with different permeability magnitudes obtained from casting thin sections and SEM. Specimens TY3 ($K_0 = 5.6 \times 10^{-17}$ m^2), TY9 ($K_0 = 2.82 \times 10^{-16}$ m^2) and TY11 ($K_0 = 1.84 \times 10^{-15}$ m^2) with permeabilities lower than 10^{-14} m^2 are all quite tight. In these specimens, the framework grains align closely leaving little space. Pores are poorly developed and connected with tiny pore throat radius (less than 1 μm). A microfracture with width smaller than 10 μm is observed in TY3, and abundant fracture-like pores and throats are visible in the three specimens (Fig. 8a, c, e). At 200× magnification under the SEM, these specimens are still extremely tight (Fig. 8b, d, f). Inversely, specimens TY16 ($K_0 = 4.91 \times 10^{-14}$ m^2), TY17 ($K_0 = 1.02 \times 10^{-13}$ m^2) and TY24 ($K_0 = 1.68 \times 10^{-12}$ m^2), whose permeabilities are larger than 10^{-14} m^2, are relatively loose. The three specimens are characterized by loosely aligned framework grains, uniformly distributed and well-connected intergranular pores, and wide throats. The pore throat radius is about 10 μm, and partial pores and throats are difficult to distinguish (Fig. 8g, i, k). Similar phenomenon can be also observed in SEM images with a magnification up to 150×

Fig. 6 Distribution of pore throat radius for samples with different porosity and permeability (The porosity and permeability were both measured under the initial confining pressure of 3 MPa.)
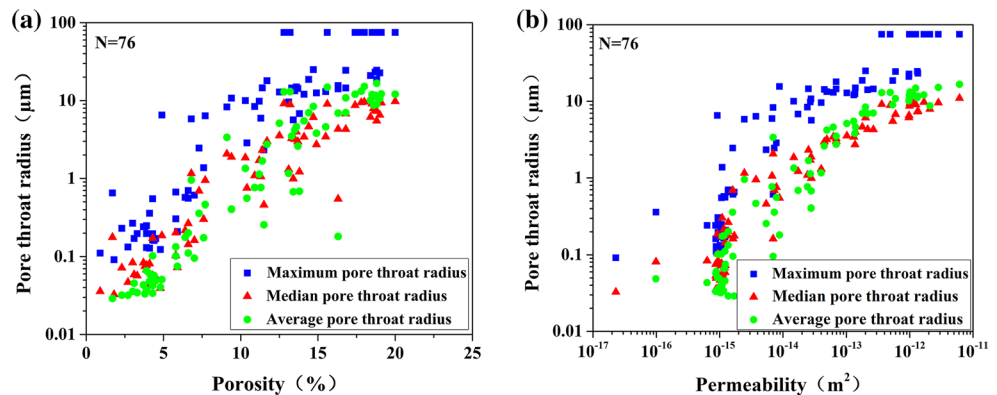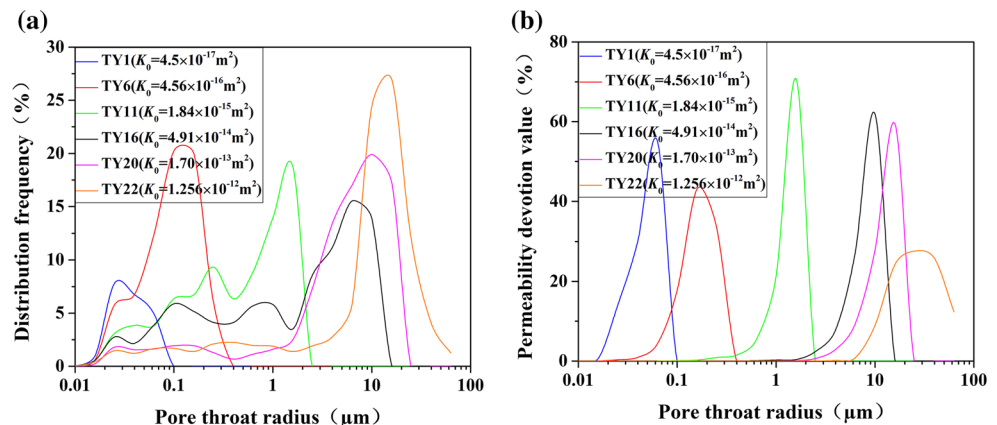

Fig. 7 Distribution of pore throat radius for specimens with different permeability
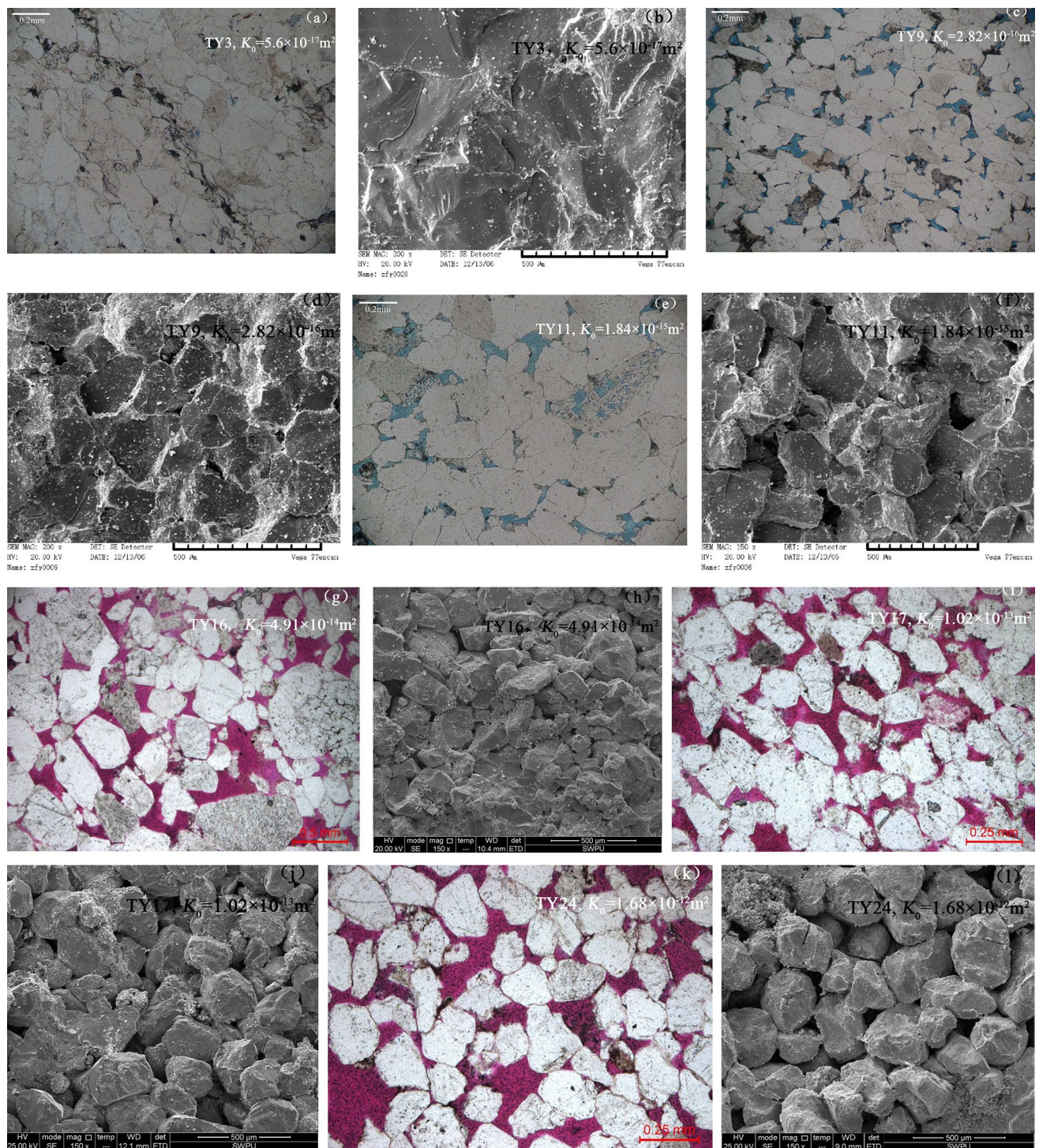
Fig. 8 Casting thin sections images and SEM images of 6 typical specimens with different permeability magnitudes: **a–b** TY3; **c–d** TY9; **e–f** TY11; **g–h** TY16; **i–j** TY17; **k–l** TY24

(Fig. 8h, j, l). In Fig. 8, the general trend is clear that the higher the permeability, the more numerous the pores, the larger the pore throat radius, the better the pore connection and the looser the structure. A pore with a smaller aspect ratio compacts more easily and keeps a smaller proportion

of its original radius under compression stress (Shar et al. 2017). The flow path in a narrow throat is almost completely closed during the loading process, while that of a wide throat is only partially closed (Tian et al. 2015a). Obviously, small pores and throats have a smaller aspect ratio than the larger

Fig. 9 Pore and throat types of clastic rock: **a** pore-shrinking throat; **b** necking throat; **c** laminated throat; **d** curved lamellar throat; **e** tube bundle-shaped throat
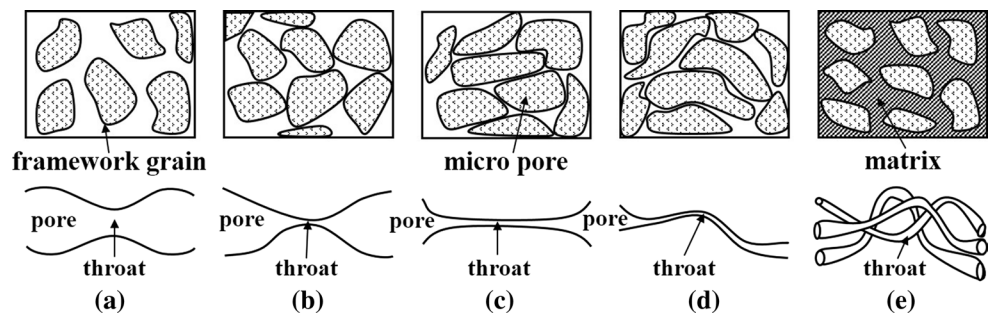
Table 3 Value of porosity sensitivity exponent and its corresponding pore and fracture structure characteristics. (Modified after Zhang et al. 2016)

α Value	The relationship between pore radius r and fracture width w	Pore and fracture structure characteristics
$\alpha < 2$	$r \gg w$	Pore dominated double-porosity system
$\alpha = 2$	$w = 0$	Kozeny capillary model
$2 < \alpha < 3$	$r \approx w$	Double-porosity system of similar sized fracture and pore
$\alpha = 3$	$r = 0$	Plate crack model
$\alpha > 3$	$r \ll w$	High fracture quantity dominated double-porosity system
$\alpha \gg 3$	$r \ll w$	Low fracture quantity dominated double-porosity system

ones. Therefore, specimen with smaller pore throat radius and greater proportion of small pore throats shows stronger stress sensitivity. That is the reason why S_s declines with increasing initial porosity and permeability and shows obvious differences on both sides of 10^{-14} m^2.

In addition to the size, the pore throat geometry also has an important influence on the stress sensitivity (Davies and Davies 2001). For Fig. 8a (TY3), c (TY9), e (TY11) with specimen permeability less than 10^{-14} m^2, the arrangement of framework gains is similar to that illustrated in Fig. 9c, d. Most throats in the three specimens are quite narrow and have similar geometry with laminated throats (Fig. 9c) and curved lamellar throats (Fig. 9d). Some local pores are completely packed by matrix and cement. Micropores inside the matrix are both a pore and a throat and are distributed across the matrix and cemented like beams of microcapillaries (tube bundle-shaped throat, Fig. 9e). In Fig. 8g (TY16), i (TY17), k (TY24) with specimen permeability larger than 10^{-14} m^2, the arrangement of framework gains is similar to that illustrated in Fig. 9a, b. Due to the loose structure of the rock, some throats are the narrow part of the pore (pore-shrinking throat), which are hard to distinguish from pores. Others are the contraction of variable section (necking throat). Pore-shrinking throats and necking throats are hard to compress due to their high aspect ratio, while laminated throats, curved lamellar throats and tube bundle-shaped throats are easy to compress due to the low aspect ratio. Therefore, lower initial permeability leads to more laminated throats, curved lamellar throats and tube bundle-shaped throats and results in stronger stress sensitivity.

4.1.3 Micro-/macro-fractures

The relation between varying permeability and porosity is described by (Faruk 2000; Petunin et al. 2011)

$$\frac{K}{K_0} = \left(\frac{\phi}{\phi_0} \right)^{\alpha} \tag{4}$$

where α is the porosity sensitivity exponent which describes the porosity–permeability relationship during effective stress loading process. By taking the logarithm of both sides of Eq. 4, α can be determined through linear regression analysis. Table 3 lists the pore and fracture structure characteristics for different α values. As α increasing from < 2 to > 3, the contribution of fractures to permeability gradually increases, while the contribution of pores decreases.

Porosity sensitivity exponent versus initial porosity and permeability is presented in Fig. 10. Specimens with lower porosity and permeability show higher α values, which indicates that the flow path in specimens with lower permeability is dominated by microfractures or fracture-like pores, while specimens with higher permeability are dominated by pores. α has a proportional relationship with S_s (Fig. 11), which indicates that the existence of microfractures can strengthen the stress sensitivity. The strengthening effect is stronger for specimens with lower permeability. A similar conclusion can also be obtained for specimens with macrofracture, as shown by the S_s values of intact and artificially fractured specimen (Fig. 4).

Fractures will significantly enhance the permeability stress sensitivity of the rock, and the stress sensitivity
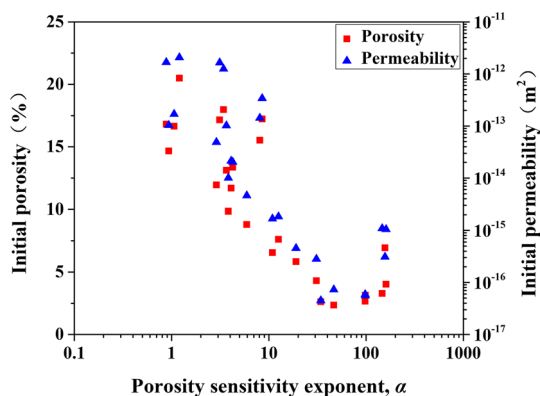
2332

C. Xu et al. (2018) 51:2321–2338

Fig. 10 Relationship of porosity sensitivity exponent with initial porosity and initial permeability
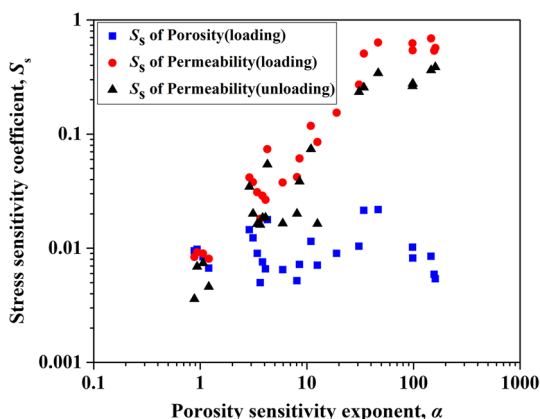

Fig. 11 Stress sensitivity coefficient vs. porosity sensitivity exponent

coefficient increases with fracture development (Xiao et al. 2016). Rock fracture density decreases with increasing confining pressure, while the proportion of pores with a high aspect ratio increases (Benson et al. 2006). The evolution of fracture density under increasing confining pressure is consistent with that of the permeability. It indicates that the main cause of permeability stress sensitivity is the closure of small aspect ratio throats and fractures, which results in the decrease in flow paths and decline in permeability.

The compressibility of a circular pore model, elliptical pore model (Zhang et al. 2015) and penny-shaped model (David et al. 1994) is adopted for numerical analysis of the effect of fractures on stress sensitivity. They are expressed in Eqs. 5–7, respectively.

$$C_c = \frac{2(1 + \nu)}{E} \tag{5}$$

$$C_e = \frac{2(1 - \nu^2)}{E}\left(\varepsilon + \frac{1}{\varepsilon}\right) \tag{6}$$

$$C_p = \frac{3(1 - 2\nu)}{E}\left[\frac{4(1 - \nu^2)}{3\pi(1 - 2\nu)\varepsilon} - 1\right] \tag{7}$$

where C_c, C_p and C_e are the compressibility of a circular pore, penny-shape pore and elliptical pore, respectively. E is the Young's modulus, and ν is the Poisson's ratio of rock. ε is the aspect ratio of pore. Young's modulus and Poison's ratio are obtained from conventional triaxial rock mechanics tests, which is 19,011.8 MPa and 0.229, respectively. The aspect range is 0.001–1, and effective stress range is 0–65 MPa. Equation 8 transformed from David et al. (1994) was used, and the right side of Eq. 8 represents the compaction ratio under effective stress loading process. When the right part approximates to 1, the pore can be considered to be closed.

$$C \cdot \Delta\sigma = -\frac{\Delta\phi}{\phi} \tag{8}$$

Numerical analysis results based on Eqs. 5–8 are shown in Fig. 12. The compressibility of elliptical pores and penny-shaped pores is significantly controlled by aspect ratio. Lower aspect ratio pores are more compressible (Fig. 12a). Figure 12b–d shows the compaction ratio with increasing effective stress. Circular pores deform only about 0.8% when stress is loaded to 65 MPa, which indicates that circular pores can hardly deform and their deformation is neglectable (Fig. 12b). For elliptical pores and penny-shaped pores, the lower the aspect ratio is, the lower the effective stress is needed to reach 100% compaction (Fig. 12c–d). These results suggest that stress sensitivity is mainly caused by pores, throats and fractures with low aspect ratio in the low effective stress range. The contribution of pore compaction is fairly limited. Lower Young's modulus leads to sharper increase in pore compressibility, while the impact of Poison's ratio is insignificant.

For rock sample under a certain stress state, fractures will be closed first, followed by throats and then the pores. This phenomenon can be explained by the shape and structure. Pores commonly have an arch structure, which has a strong resistance to collapse under stress and is hard to deform. Throats have a counter-arched structure, which makes them easier to deform and leads to decreasing throat radius. Fractures usually have an extremely small aspect ratio. Abundant asperities with different sizes and shapes are distributed on the fracture surface. The asperities on the two fracture faces do not fully match each other, which leaves a flow path. These make fracture are more prone to be closed under compression.
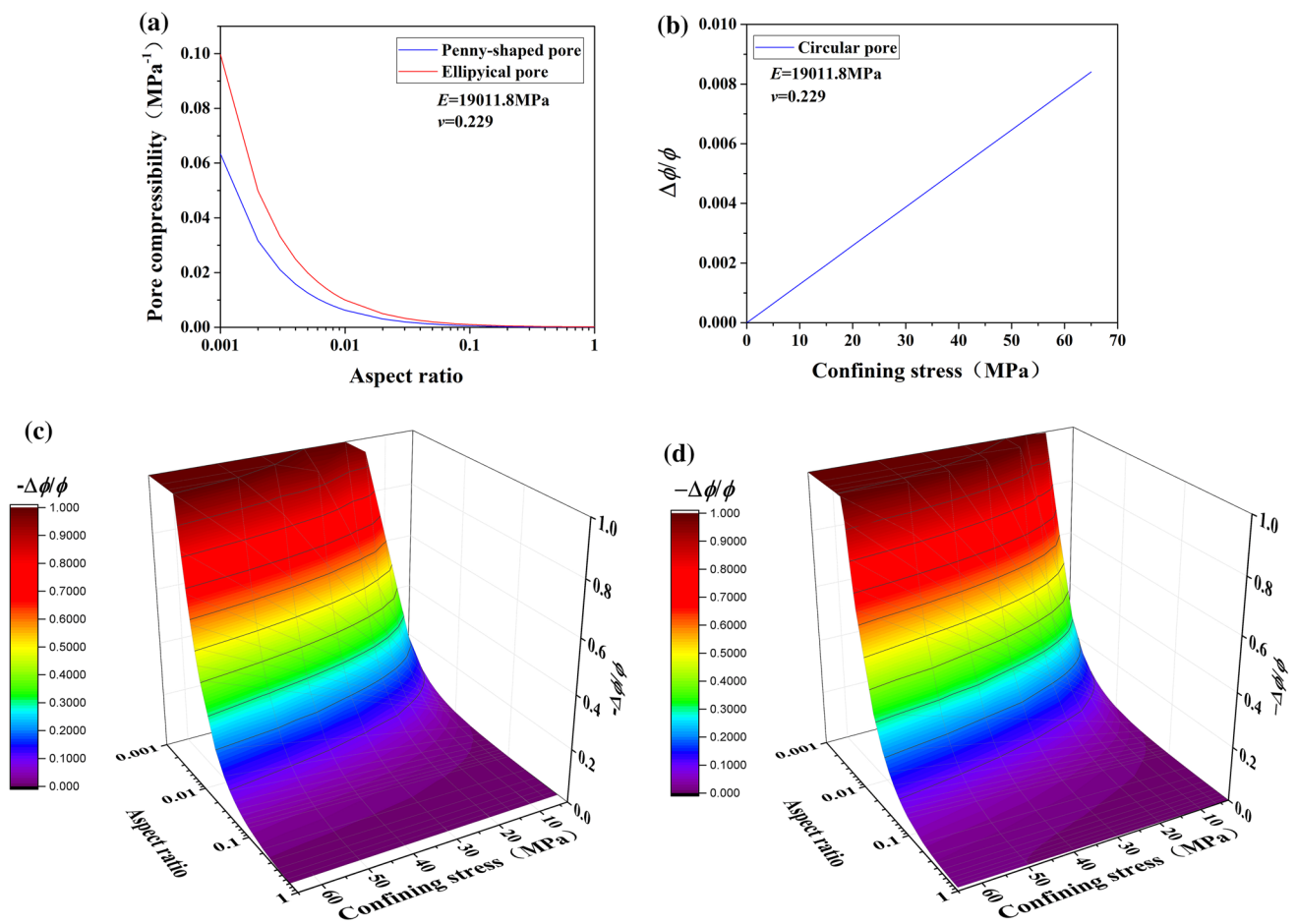
Fig. 12 Numerical analysis results of pore compaction under confining stress: **a** pore compressibility versus pore aspect ratio; **b** the compaction ratio vs. confining stress for a circular pore; **c** the compaction ratio versus confining stress and aspect ratio for penny-shaped pores; **d** the compaction ratio versus confining stress and aspect ratio for elliptical pores

4.1.4 Interstitial Materials

Interstitial materials are those materials filling in the pores or spaces between the framework grains. The interstitial materials can support the pores, throats and microfractures and affect the deformation of rock (Tian et al. 2015a). It is well known that hard materials are harder to compress while soft ones are easier. The hardness of common minerals from high to low is: quartz, feldspar, calcite, mica and clay minerals. The bulk modulus of quartz, calcite, dolomite and pyrite are quite larger than those of clay minerals, such as kaolinite (Table 4). The measured bulk modulus of pure clay is reported about 3–6 times less than that of quartz (Vanorio et al. 2003), and the elastic deformation of clays is reported

to be 25 times more than quartz (Farber et al. 2001). Once loaded, clay minerals contribute the major deformation of sandstone after closure of void space due to their platy-like structures and low elastic modulus (Al-Wardy and Zimmerman 2004; Kopycinska-Müller et al. 2007). Developed clay mineral is an indication of higher sensitivity to stress (Bustin et al. 2008). Thin section analysis results show that experimental sandstone samples with higher permeability ($K \geq 10^{-14}$ m^2) have similar content of interstitial materials to samples with lower permeability ($K < 10^{-14}$ m^2). However, lower permeability samples have higher matrix (mainly clay) content (Table 5). In spite of the small total soft minerals content, lower permeability specimens show much stronger stress sensitivity. It is because that although

Table 4 Bulk modulus of minerals. (Reproduced with permission from Anderson and Isaak 1995; Jay 1995; Vanorio et al. 2003)

Mineral	Quartz	Calcite	Dolomite	Pyrite	Kaolinite	Clay
Bulk modulus (GPa)	37.8	73.3	94.9	142.7	11	6–12

Table 5 Framework components and interstitial material of experimental sandstone samples

Permeability range	S_s	Framework components (%)				Interstitial material (%)							
		Quartz	Feldspar		Detritus	Total	Matrix	Cement					
			Potassium feldspar	Anorthose				Total	Calcite	Ferrocalcite	Siliceous	Kaolinite
$\geq 10^{-14}$ m^2	0.04–0.70 / 0.41	87–89 / 87.75	–	–	11–13 / 12.25	3–5 / 4.50	1–1 / 1	2–4 / 3.50	<1	<1	1–2 / 1.75	1–2 / 1.75
$< 10^{-14}$ m^2	0.01–0.03 / 0.08	75–88 / 83.14	<1	<1	11–25 / 16.71	3–6 / 4.29	1–4 / 1.71	1–4 / 2.57	–	–	1–4 / 2.43	–

The number above the underline is the range of values while the number below the underline is the average

the small total soft minerals content, their relative proportion of soft minerals to pore space in lower permeability specimen is larger due to tiny and complex microstructure, which results in stronger throats deformation and permeability stress sensitivity (Tian et al. 2015a). Furthermore, detritus content of lower permeability samples is higher than that in higher permeability samples, which also leads to stronger stress sensitivity.

4.2 Mechanical Mechanisms of Sandstone Stress-Sensitive Behavior

The stress sensitivity of rock porosity and permeability is a result of flow path change which is caused by deformation under variable stress. The deformation includes body deformation and structural deformation. Body deformation is the deformation of rock framework grains, while structural deformation is the pore deformation due to the arrangement change in rock framework grains. The deformation of specimen is related to the elastic closure of microfractures initially and relative movement of framework grains later, without grain crushing or pore collapse (David et al. 1994). If we assume representative elastic moduli values for quartz ($E = 40$–150 GPa and $\nu = 0.3$), then its coefficient of compressibility can be estimated as 3×10^{-5}–8×10^{-6} MPa^{-1}. It is orders of magnitude less than that of pore calculated by Eqs. 5–7, which is 2×10^{-7}–6×10^{-2} MPa^{-1} (aspect ratio within 0.001–1). This is consistent with the observation of McKee et al. (1988) and Tiab and Donaldson (1996) that compressibility of grains is negligible compared to that of porosity in low permeable sandstone and shale. Therefore, accounting for the analysis of Sect. 4.1.4, it can be concluded that body deformation of the tested sandstone specimens is unimpressive and mainly comes from the agglutinate and interstitial materials under the above-mentioned experimental conditions. That is, the structural deformation is the controlling factor of sandstone stress sensitivity.

Rock deformation properties are controlled by rock structure and mineral composition. Different mineral compositions, pores, throats and microfractures do not deform uniformly under uniform stress. Therefore, their contribution to permeability variation is also different. The rock deformation and corresponding permeability evolution of sandstone specimens under increasing stress can be divided into three stages (Fig. 13). Stage I (0–10 MPa) is the permeability rapid decline phase. In this stage, microfractures, fracture-like pores and throats (all these void spaces are characterized by a small aspect ratio) are closed under the effective stress. As shown in Fig. 12, the smaller the aspect ratio of a pore, the lower stress the pore needs to be closed. Due to the important contribution of these void spaces to the permeability, especially for some lower permeability specimens, the permeability loss in this stage accounts for most of the total permeability loss. At the end of this stage, the microfracture flow changes to pore flow. Stage II (10–20 MPa) is the permeability moderative decline phase. After the closure of microfractures, fracture-like pores and throats in stage I, the relatively soft minerals distributed on the sand surface, including detritus, argillaceous cement and clays, come into contact. These soft minerals are compacted by the rising effective stress because of their higher compressibility compared to quartz. As a result, the flow space in a clay laminated structure is reduced and permeability continues to decline. Due to the weaker compressibility related to microfractures, fracture-like pores and throats and continuous closure of flow space, the permeability decrease rate declines. Stage III (20–65 MPa) is the permeability stable-slight decline phase. As the stronger compressibility pore and minerals have been compacted, quartz grains now begin to deform. Because compaction and relative movement of quartz grain are hard to occur before crushing and the seepage process of sandstone is mainly pore flow, the permeability declines slightly. For the artificially fractured specimen and some specimens (TY1, TY2, TY3, TY4, TY5, TY7 and TY8) with permeability less than 10^{-14} m^2, the three stages can be manifestly distinguished (Fig. 3a–c, g) due to the existence of a certain amount of micro-/macro-fractures, fracture-like pores and narrow throats (Fig. 8a–f). Stress sensitivity of these specimens is mainly dominated by stage I, during which over 70% of the initial permeability is lost, which indicates a strong

Fig. 13 Sketch on three stages characterizing the evolution of permeability of sandstone in effective stress loading
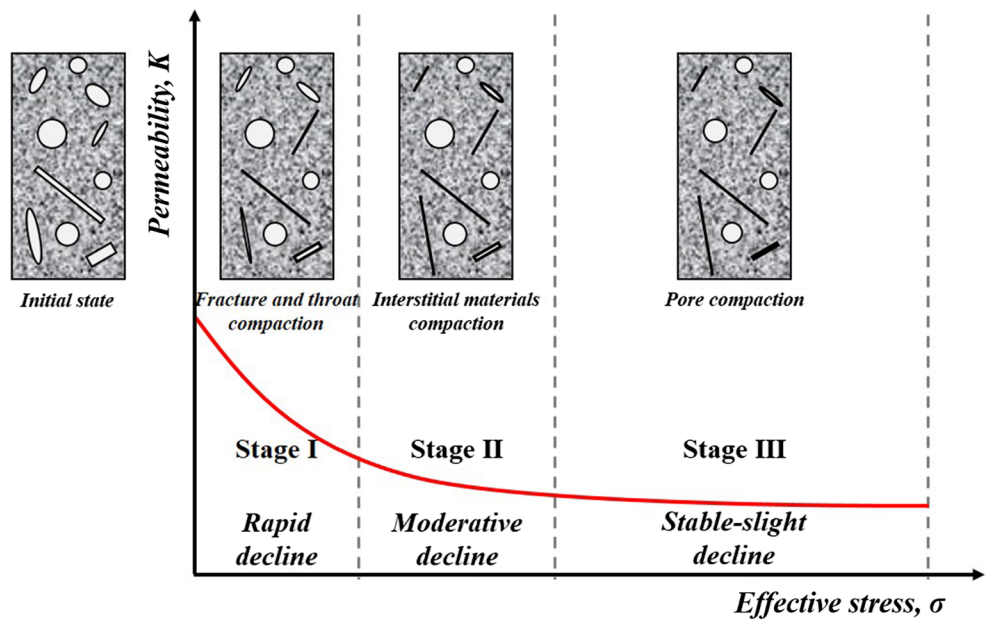

stress sensitivity. On the other hand, the three stages for the rest specimens are unapparent (Fig. 3d–f), because they are mainly composed by pores and wide throats (Fig. 8g–l). Stress sensitivity of these specimens is the result of all the three stages and only a small percentage of the initial permeability is lost, which indicates the weak stress sensitivity.

4.3 Comparison Between Laboratory-Scale and Field-Scale Stress-Sensitive Behavior

All specimens used in stress sensitivity tests experienced long-term stress relaxation compared to its in situ status. As a result, void space increases due to the opening of

compacted fractures, throats and pores. The induced micro-fracture generated in the coring and cutting process can also enhance the stress sensitivity of the specimen (Spencer 1989). This may contribute most to the rapid decrease in permeability under low effective stress. In addition, the effective stress change in the laboratory is larger than that in real exploration and development (Tian 2014). The rapid decline stage under low effective stress seldom exists in situ state. The stress sensitivity of porosity and permeability is usually overestimated in laboratory conditions (Fig. 14). The impact of stress sensitivity on oil and gas exploration and development is probably not that much. What is more, the stress state, temperature, fluid saturation, flowing fluid and

Fig. 14 Effective stress variation ranges comparison between the laboratory and a real reservoir

2336

C. Xu et al. (2018) 51:2321–2338
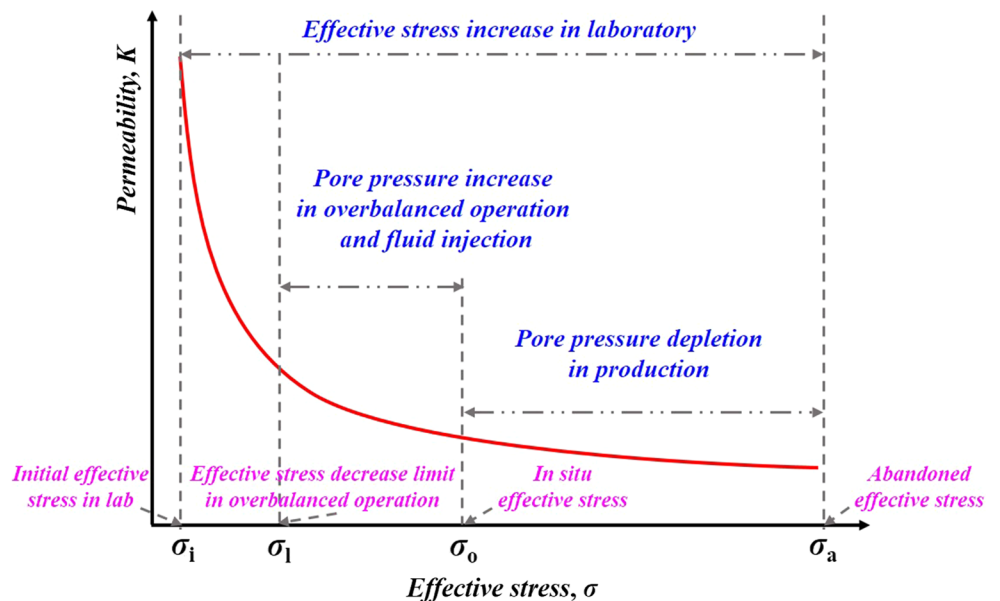
external fluid effects, which cause errors in stress sensitivity evaluation, are all quite different between the laboratory and the reservoir conditions. Therefore, for accurate analysis of reservoir stress-sensitive behavior, the specimen preparation and the experimental conditions need to be as close as possible to the reservoir condition.

5 Conclusions

Porosity and permeability stress sensitivity tests are conducted on 27 sandstone specimens from the Silurian Formation of Tarim Basin in northwestern China. The stress-sensitive behavior is analyzed, and the stress sensitivity is evaluated using the empirical logarithm model. The microstructure of sandstone is observed through mercury injection, casting thin sections and SEM. Controlling factors and mechanisms of stress sensitivity are discussed according to the relationship of stress sensitivity and microstructure observation results. Differences in stress-sensitive behavior between laboratory-scale and field-scale settings are discussed.

Both the porosity and permeability continuously decline with increasing effective stress. The experimental data obey the empirical logarithmic model quite well. The stress sensitivity coefficient is negatively related to the initial porosity and permeability of the specimen, while permeability recovery rate is positively related to these two parameters. Two demarcation points (10% for initial porosity and 10^{-14} m^2 for initial permeability) are observed in permeability stress sensitivity, below which the permeability stress sensitivity is significantly higher and the permeability recovery rate is much lower. Permeability stress-sensitive behavior is mainly controlled by the size and shape of microscopic pores, throats, fractures and the mechanical properties of minerals. The compaction and closure of the throats and fractures are the most important reasons for sandstone stress sensitivity. Pores and throats with a smaller aspect ratio and irregular shapes, developed fractures and more soft minerals lead to stronger stress sensitivity of sandstone. Stress sensitivity evaluated in the laboratory conditions is not completely representative of that in a reservoir condition due to stress relief, drilling induced fractures and environmental deviations. For a more accurate investigation, actual reservoir conditions need to be simulated as much as possible.

References

Al-Wardy W, Zimmerman RW (2004) Effective stress law for the permeability of clay-rich sandstones. J Geophys Res 109(B04203):1–10

Anderson OL, Isaak DG (1995) Elastic constants of mantle minerals at high temperature. In: Ahrens TJ (ed) Mineral physics and crystallography: a handbook of physical constants. American Geophysical Union, Washington DC, pp 64–97

Archer RA (2008) Impact of stress sensitive permeability on production data analysis. In: SPE unconventional reservoirs conference, 10–12 Feb, Keystone

Benson P, Schubnel A, Vinciguerra S, Trovato C, Meredith P, Young RP (2006) Modeling the permeability evolution of microcracked rocks from elastic wave velocity inversion at elevated isostatic pressure. J Geophys Res 111(B04202):1–11

Bernabé Y, Mok U, Evans B (2003) Permeability-porosity relationships in rocks subjected to various evolution processes. Pure appl Geophys 160(5):937–960

Berumen S and Tiab D (1996) Effect of pore pressure on conductivity and permeability of fractured rocks. In: SPE western regional meeting, 22–24 May, Anchorage

Brower KR, Morrow NR (1985) Fluid flow in cracks as related to low-permeability gas sands. SPE J 25(2):191–201

Bruno MS, Bovberg CA, Nakagawa FM (1991) Anisotropie stress influence on the permeability of weakly-cemented sandstones. In: The 32nd US symposium on rock mechanics (USRMS), 10–12 July, Norman

Bustin A, Bustin RM, Cui XJ (2008) Importance of fabric on the production of gas shales. In: SPE unconventional reservoirs conference, 10–12 Feb, Keystone

Clarkson CR, Jensen JL, Pedersen PK, Freeman M (2012) Innovative methods for flow-unit and pore-structure analyses in a tight siltstone and shale gas reservoir. AAPG Bull 96(2):355–374

Dautriat J, Gland N, Youssef S, Rosenberg E, Bekri S, Vizika O (2009) Stress-dependent directional permeabilities of two analog reservoir rocks: a prospective study on contribution of μ-tomography and pore network models. SPE Reserv Eval Eng 12(2):297–310

David C, Wong TF, Zhu WL, Zhang JX (1994) Laboratory measurement of compaction-induced permeability change in porous rocks: implications for the generation and maintenance of pore pressure excess in the crust. Pure appl Geophys 143(1–3):425–456

Davies JP, Davies DK (2001) Stress-dependent permeability: characterization and modeling. SPE J 6(2):224–235

Dong JJ, Hsu JY, Wu WJ, Shimamoto T, Hung JH, Yeh EC, Wu YH, Sone H (2010) Stress-dependence of the permeability and porosity of sandstone and shale from TCDP Hole-A. Int J Rock Mech Min Sci 47(7):1141–1157

Dormieux L, Jeannin L, Gland N (2011) Homogenized models of stress-sensitive reservoir rocks. Int J Eng Sci 49(5):386–396

Farber DL, Bonner BP, Balooch M, Viani B, Siekhaus W (2001) Observations of a water induced transition from brittle to viscoelastic behavior in nanocrystalline swelling clay. In: AGU fall meeting 2001, 10–14 Dec, San Francisco

Farquhar RA, Smart B, Todd AC, Tompkins DE, Tweedie AJ (1993) Stress sensitivity of low-permeability sandstones from the Rotliegendes sandstone. In: SPE annual technical conference and exhibition, 3–6 Oct, Houston

Faruk C (2000) Predictability of porosity and permeability alterations by geochemical and geomechanical rock and fluid interactions. In: SPE international symposium on formation damage control, 23–24 Feb, Lafayette

Fatt I, Davis DH (1952) Reduction in permeability with overburden pressure. Pet Trans AIME 195:329

Fu X, Agostini F, Skoczylas F, Jeannin L (2015) Experimental study of the stress dependence of the absolute and relative permeabilities of some tight gas sandstones. Int J Rock Mech Min Sci 77:36–43

Geertsma J (1957) The effect of fluid pressure decline on volumetric changes of porous rocks. Pet Trans AIME 210:331–340

Ghabezloo S, Sulem J, Guédon S, Martineau F (2009) Effective stress law for the permeability of a limestone. Int J Rock Mech Min Sci 46(2):297–306

Han B, Xie SY, Shao JF (2016) Experimental investigation on mechanical behavior and permeability evolution of a porous limestone under compression. Rock Mech Rock Eng 49(9):3425–3435

Huo D, Li B, Benson SM (2014) Investigating aperture-based stress-dependent permeability and capillary pressure in rock fractures. In: SPE annual technical conference and exhibition, 27–29 Oct, Amsterdam

Jaeger JC, Cook NG, Zimmerman R (2007) Fundamentals of rock mechanics, 4th edn. Wiley, Hoboken

Jay D (1995) Elasticity of Minerals, Glasses, and Melts. In: Ahrens TJ (ed) Mineral physics and crystallography: a handbook of physical constants. American Geophysical Union, Washington DC, pp 45–63

Jones FO, Owens WW (1980) A laboratory study of low-permeability gas sands. J Pet Technol 32(9):1631–1640

Kang YL, Xu CY, You LJ, Tang L, Lian ZH (2015) Comprehensive prediction of dynamic fracture width for formation damage control in fractured tight gas reservoir. Int J Oil Gas Coal T 9(3):296–310

Kang YL, She JP, Zhang H, You LJ, Yu YF, Song MG (2016) Alkali erosion of shale by high-pH fluid: reaction kinetic behaviors and engineering responses. J Nat Gas Sci Eng 29:201–210

Kassis SM and Sondergeld CH (2010) Fracture permeability in the Barnett shale: effects of roughness, fracture offset, proppant, and effective stress. In: International oil and gas conference and exhibition in China, 8–10 June, Beijing

Kilmer NH, Morrow NR, Pitman JK (1987) Pressure sensitivity of low permeability sandstones. J Pet Sci Eng 1(1):65–81

Kopycinska-Müller M, Prasad M, Rabe U, Arnold W (2007) Elastic properties of clay minerals determined by atomic force acoustic microscopy technique. In: André MP (ed) Acoustical imaging, vol 28. Springer, Dordrecht, pp 409–416

Lei Q, Xiong W, Yuan JR, Cui YQ, Wu YS (2008) Analysis of stress sensitivity and its influence on oil production from tight reservoirs. In: SPE eastern regional meeting, 17–19 Oct, Lexington

Li S, Tang DZ, Pan ZJ, Xu H, Huang WQ (2013) Characterization of the stress sensitivity of pores for different rank coals by nuclear magnetic resonance. Fuel 111(3):746–754

Li XC, Kang YL, Chen DF (2017a) Effect of fracturing fluid on coal-bed-methane desorption, diffusion, and seepage in the Ningwu Basin of China. SPE Prod Oper 32(2):177–185

Li X, Feng ZJ, Han G, Elsworth D, Marone C, Saffer D, Cheon DS (2017b) Permeability evolution of propped artificial fractures in Green River shale. Rock Mech Rock Eng 50(6):1473–1485

Liu L, Xu WY, Wang HL, Wang W, Wang RB (2016) Permeability evolution of granite gneiss during triaxial creep tests. Rock Mech Rock Eng 49(9):3455–3462

Louis C (1972) Rock hydraulics. In: Müller L (ed) Rock mechanics. Springer, Vienna, pp 299–387

Ma JJ, Wang J (2016) A stress-induced permeability evolution model for fissured porous media. Rock Mech Rock Eng 49(2):477–485

Mckee CR, Bumb AC, Koenlg RA (1988) Stress-dependent permeability and porosity of coal and other geologic formations. SPE Form Eval 3(1):81–91

Meng Y, Li ZP, Lai FP (2015) Experimental study on porosity and permeability of anthracite coal under different stresses. J Pet Sci Eng 133:810–817

Nguyen VH, Gland N, Dautriat J, David C, Wassermann J, Guélard J (2014) Compaction, permeability evolution and stress path effects in unconsolidated sand and weakly consolidated sandstone. Int J Rock Mech Min Sci 67:226–239

Ostensen RW (1983) Microcrack permeability in tight gas sandstone. SPE J 23(6):919–927

Ostensen RW (1986) Effect of stress-dependent permeability on gas production and well testing. SPE Form Eval 1(3):227–235

Petunin VV, Yin X, Tutuncu AN (2011) Porosity and permeability changes in sandstones and carbonates under stress and their correlation to rock texture. In: Canadian unconventional resources conference, 15–17 Nov, Calgary

Qi T, Sun JC, Yang ZM (2013) Comparative study on stress-dependent permeability of ultra-low permeability sandstone rock using different types of fluid media. In: International petroleum technology conference, 26–28 March, Beijing

Santos ESR, Borba AM, Ferreira FH (2014) Stress-dependent permeability measurement of Indiana limestone and Silurian dolomite samples in hydrostatic tests. In: ISRM conference on rock mechanics for natural resources and infrastructure—SBMR 2014, 9–13 Sept, Goiania

Seeburger DA, Amos N (1984) Pore space model for rock permeability and bulk modulus. J Geophys Res 89(B1):527–536

Shapiro SA, Niemann R, Khizhniak GP, Ilyushin PY, Plotnikov VV, Galkin SV (2015) Stress-dependent permeability versus stiff and compliant porosity: theory and experiments. In: 2015 SEG annual meeting, 18–23 Oct, New Orleans

Shar AM, Mahesar AA, Chandio AD, Memon KR (2017) Impact of confining stress on permeability of tight gas sands: an experimental study. J Pet Explor Prod Technol 7(3):717–726

Shi YL, Wang CY (1986) Pore pressure generation in sedimentary basins: overloading versus aquathermal. J Geophys Res 91(B2):2153–2162

Spencer CW (1989) Review of characteristics of low-permeability gas reservoirs in Western United States. AAPG Bull 73(5):613–629

Thomas RD, Ward DC (1972) Effect of overburden pressure and water saturation on gas permeability of tight sandstone cores. J Pet Technol 24(2):120–124

Tiab D, Donaldson EC (1996) Petrophysics: theory and practice of measuring reservoir rock and fluid transport properties. Gulf Publishing Company, Houston

Tian Y (2014) Experimental study on stress sensitivity of naturally fractured reservoirs. In: SPE annual technical conference and exhibition, 27–29 Oct, Amsterdam

Tian XF, Cheng LS, Cao RY, Wang Y, Zhao WQ, Yan YQ, Liu HJ, Mao WH, Zhang MY, Guo Q (2015a) A new approach to calculate permeability stress sensitivity in tight sandstone oil reservoirs considering micro-pore-throat structure. J Pet Sci Eng 133:576–588

Tian XF, Cheng LS, Yan YQ, Liu HJ, Zhao WQ, Guo Q (2015b) An improved solution to estimate relative permeability in tight oil reservoirs. J Pet Explor Prod Technol 5(3):305–314

Vairogs J, Hearn CL, Dareing DW, Rhoades VW (1971) Effect of rock stress on gas production from low-permeability reservoirs. J Pet Technol 23(9):1161–1167

Vanorio T, Prasad M, Nur A (2003) Elastic properties of dry clay mineral aggregates, suspensions and sandstones. Geophys J Int 155(1):319–326

Vogler D, Amann F, Bayer P, Elsworth D (2016) Permeability evolution in natural fractures subject to cyclic loading and gouge formation. Rock Mech Rock Eng 49(9):3463–3479

Walsh JB (1981) Effect of pore pressure and confining pressure on fracture permeability. Int J Rock Mech Min Sci Geomech Abstr 18(5):429–435

Wang HL, Xu WY, Cai M, Xiang ZP, Kong Q (2017) Gas permeability and porosity evolution of a porous sandstone under repeated loading and unloading conditions. Rock Mech Rock Eng 50(8):2071–2083

Worthington PF (2008) A diagnostic approach to quantifying the stress sensitivity of permeability. J Pet Sci Eng 61(2–4):49–57

Xiao WL, Li T, Li M, Zhao JZ, Zheng LL, Li L (2016) Evaluation of the stress sensitivity in tight reservoirs. Pet Explor Dev 43(1):115–123

Xu P, Yang SQ (2016) Permeability evolution of sandstone under short-term and long-term triaxial compression. Int J Rock Mech Min Sci 85:152–164

Xu CY, Kang YL, You ZJ, Chen MJ (2016) Review on formation damage mechanisms and processes in shale gas reservoir: known and to be known. J Nat Gas Sci Eng 36:1208–1219

Xu CY, Kang YL, You LJ, You ZJ (2017) Lost circulation control for formation damage prevention in naturally fractured reservoir: mathematical model and experimental study. SPE J 22(5):1654–1670

Xu CY, You ZJ, Kang YL, You LJ (2018) Stochastic modelling of particulate suspension transport for formation damage prediction in fractured tight reservoir. Fuel 221:476–490

Yang DS, Wang W, Chen WZ, Wang SG, Wang XQ (2017) Experimental investigation on the coupled effect of effective stress and gas slippage on the permeability of shale. Sci Rep 7:44696

Zhang CL (2013) Sealing of fractures in claystone. J Rock Mech Geotech Eng 5(3):214–220

Zhang HY, Liu HQ, Luan GH, He SL, Gu DH, Mo SY, Lei G (2014) A novel quantitative petrophysical model for the stress sensitivity of tight sandstones. J Pet Sci Eng 122:657–666

Zhang R, Ning ZF, Yang F, Wang X, Zhao HW (2015) Impacts of nanopore structure and elastic properties on stress-dependent permeability of gas shales. J Nat Gas Sci Eng 26:1663–1672

Zhang R, Ning ZF, Yang F, Zhao HW, Wang Q (2016) A laboratory study of the porosity-permeability relationships of shale and sandstone under effective stress. Int J Rock Mech Min Sci 81:19–27

Zheng JT, Zheng LG, Liu HH, Ju Y (2015) Relationships between permeability, porosity and effective stress for low-permeability sedimentary rock. Int J Rock Mech Min Sci 78:304–318